Biochimica et Biophysica Acta, 977 (1989) 273–286
Elsevier

BBABIO 43067

A superexchange mechanism for the primary charge separation in photosynthetic reaction centers

M. Bixon [1], Joshua Jortner [1], M.E. Michel-Beyerle [2] and A. Ogrodnik [2]

[1] *School of Chemistry, Raymond and Beverly Sackler Faculty of Exact Sciences, Tel-Aviv University, Tel-Aviv (Israel)* and [2] *Institut für Physikalische und Theoretische Chemie, Technische Universität München, Garching, (F.R.G.)*

(Received 27 February 1989)
(Revised manuscript received 19 June 1989)

Key words: Superexchange mechanism; Reaction center; Photosynthesis; Charge separation; Quantum mechanics; Franck-Condon factor

We analyse the superexchange model for the primary charge separation from the electronically excited singlet state ($^1P^*$) of the bacteriochlorophyll dimer (P) to the bacteriopheophytin (H) across the A branch of the bacterial photosynthetic reaction centers, which is mediated by the accessory bacteriochlorophyll (B). The dominant contribution to the superexchange electronic interaction between the initial $^1P^*BH$ and the final P^+BH^- states originates from the mixing with the mediating electronic state P^+P^-H, the energy of which is above $^1P^*$. The superexchange electronic interaction is $V = V_{PB}V_{BH}/\delta E$, where V_{PB} and V_{BH} are the electronic couplings of $^1P^*BH$ with P^+B^-H and P^+B^-H with P^+BH^-, respectively, while δE is the vertical energy difference. The nonadiabatic electron-transfer rate is proportional to V^2F, where F is the nuclear Franck-Condon factor, which is determined by the (free) energy gap $\Delta G = -2000$ cm^{-1}, the medium reorganization energy λ ($\lambda < 2500$ cm^{-1}) and the medium characteristic frequency $\omega \approx 100$ cm^{-1}. Indirect information on the constituents of the effective electronic coupling $V \approx 25$ cm^{-1} was inferred from the ratio $|V_{BH}/V_{PB}|$ calculated from the intermolecular overlap approximation in conjunction with an activated sequential channel and the utilization of kinetic constraints on the dynamics of the primary electron transfer, which result in $V_{PB} \geq 60$ cm^{-1}, $V_{BH} \geq 360$ cm^{-1} and $\delta E \geq 1100$ cm^{-1}. We discuss several physical phenomena and observables, i.e., electric field effects on the prompt fluorescence, the unidirectionality of charge separation across the A branch and magnetic interactions in the primary radial pair in the framework of the superexchange mechanism. The electric field (ϵ) dependence of the fluorescence quantum yield ($Y_f(\epsilon)$) for isotropic samples at 75 K predicts $Y_f(\epsilon = 5$ mV/Å$)/Y_f(0) = 1.39$ and $Y_f(\epsilon = 9$ mV/Å$)/Y_f(0) = 3.5$. The fluorescence polarization data at constant field (Lockhart, D.J., Goldstein, R.F. and Boxer, S.G. (1988) J. Chem. Phys. 89, 1408–1415) can be well accounted for in terms of the energetic parameters $\lambda = 1600$ cm^{-1} and $\Delta G = -2000$ cm^{-1} together with the value $\psi = 61°$ for the angle between the dipole P^+H^- and the transition moment of P. The unidirectionality of the charge separation across the A branch originates predominantly from structural symmetry breaking, which affects the electronic coupling, while the contribution of the nuclear contribution has been shown to be small. The predicted ratio of the electronic transfer rates $k(A)/k(B) = 82(+190; -70)$ at $T = 80$ K is consistent with the recent experimental result $k(A)/k(B) \geq 25$ at this temperature. Finally we examined magnetic interactions of the primary P^+H^- radical pair, establishing the interrelationship between the singlet energy shifts and the triplet energy shift with the primary electron transfer rate, k, and the triplet recombination rate k_T whereupon the singlet-triplet splitting of P^+H^- is $J = \alpha k - \beta k_T$ where the coefficients α and β depend on energetic parameters and Franck-Condon factors. The estimate of J within the superexchange mechanism rests on the incorporation of an assumed configurational relaxation and essential cancellation effects.

Introduction

The first steps in photosynthesis of purple bacteria involve the absorption of light in antenna pigments and excitation transfer to a specialized, membrane-bound pigment-protein complex, i.e., the reaction center (RC).

Abbreviations: RC, reaction centre; P, bacteriochlorophyll dimer; H, bacteriopheophytin; $^1P^*$, electronically excited singlet state of P to H; B, accessory bacteriochlorophyll; F, Franck-Condon factor.

Correspondence: J. Jortner, School of Chemistry, Raymond and Beverly Sackler Faculty of Exact Sciences, Tel-Aviv University, 69978 Tel-Aviv, Israel.

The X-ray structure analysis was first performed on RCs of *Rhodopseudomonas viridis* [1–3] and more recently extended to RCs of *Rhodobacter sphaeroides*, strain R-26 [4–7]. The principal features of the ordering of cofactors along two almost symmetrical branches, A and B, are the same for the two species. In both cases two bacteriochlorophyll molecules are positioned very close to the approximate twofold rotation axis and are characterized by a short center-to-center distance of approx. 7 Å, thus forming the 'special pair' (P) [8,9]. Next to the special pair components, P_A and P_B, are the accessory bacteriochlorophyll monomers (B) followed in each branch by a bacteriopheophytin (H) molecule. The sequence of prosthetic groups in the two branches is terminated by quinones (Q) structurally connected by non-heme bound Fe^{2+}.

One of the most challenging problems in bacterial photosynthesis is the mechanism of the primary electron transfer from $^1P^*$ to the first spectroscopically resolved acceptor species H. This electron transfer spanning a center-to-center distance of 17 Å is extremely fast with a time constant of several picoseconds [10,11] and is strongly unidirectional along the A-branch. Recent femtosecond time-resolved spectroscopy on RCs of both *Rb. sphaeroides* [12] and *Rps. viridis* [13] has revealed a rate of $(3.6 \pm 0.2) \cdot 10^{11}\ s^{-1}$ at 295 K for both species which increases upon lowering the temperature to 10 K by factors of 2 and 4, respectively [14,15]. Most surprisingly, all changes observed between 500 nm and the Q_y transition of P occur with the same time constant [12–15]. This implies that there is no experimental indication of the B monomer being a kinetic intermediate in the first electron transfer step, in spite of its location between the donor $^1P^*$ and the acceptor H. This conclusion is also substantiated by other ps- and fs-absorption measurements, e.g., Ref. 16. On the other hand, these experiments do not allow us to rule out a priori a situation where such an intermediate P^+B^- ion pair is in fact formed with the measured rate k but at the same time depleted with a rate constant k_2 which is fast as compared to the k. The low-temperature measurements yield a lower limit for the hypothetical ratio $k_2/k \geq 70$ [14,15].

For the explanation of the fast primary electron transfer between $^1P^*$ and H several mechanisms were considered [17,91]. Among these, sequential mechanisms [18–21], nonadiabatic-adiabatic mechanisms [17,22] as well as a unistep superexchange mechanism [23–33] were invoked. In the latter mechanism the electronic coupling between the donor $^1P^*$ and the acceptor H is not only due to the direct coupling but is enhanced by mixing with a state P^+S^-H (or PS^+H^-) involving a species S located between P and H. Although there are some experimental findings [27,28,34–36] pointing against sequential mechanisms and towards the applicability of superexchange, we will not go into the details of such arguments but rather concentrate throughout this paper on the description of the unistep superexchange model.

The importance of the superexchange interaction is that it adds to the weak direct electronic coupling between donors and acceptors separated by a large distance. If in this case a bridging molecule (S) with appropriate orbitals can be introduced between donor (D) and acceptor (A), its electronic states can enhance the coupling by mixing with the donor or acceptor states. The effective coupling between a donor 1 and an acceptor 3 is then the sum of the direct coupling and the superexchange coupling, V_{super}, mediated by a state 2, (D^+S^- or S^+A^-), which in first order perturbation is given by

$$V_{super} = \frac{V_{12}V_{23}}{\delta E_{12}} \tag{1}$$

V_{12} and V_{23} are the electronic coupling between the corresponding states and δE_{12} is the vertical energy gap between state 1 and 2 at the configuration of the intersection of the potential energy surfaces of states 1 and 3 (Fig. 1). The value of V_{super} thus results from the interplay between the couplings and the energy gap.

The idea of superexchange first appeared when Kramers [37] tried to understand the early adiabatic demagnetization results in paramagnetic salts, which indicated that small exchange couplings existed even between ions separated by one or several diamagnetic groups. He pointed out that the ions could cause spin-dependent perturbations in the wavefunctions of intervening ions, thereby transmitting the exchange effect over large distances which led to the name 'superex-

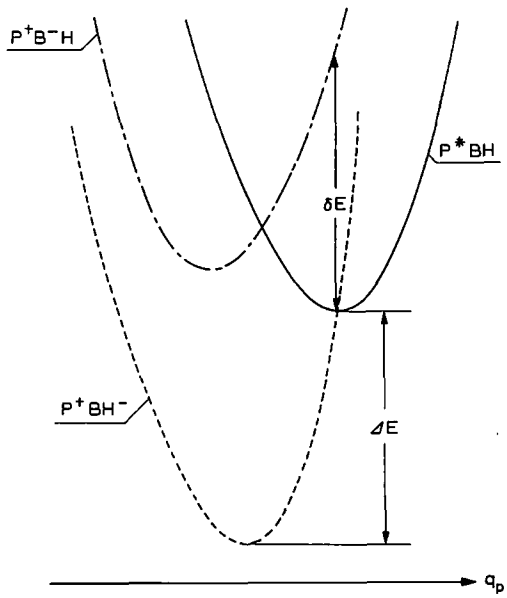

Fig. 1. Nuclear potential energy surfaces for the superexchange electronic interaction mechanism in the RC.

change' [38]. The concept was revived and extended by Anderson [39] and applied by McConnel [40] to explain magnetic interactions in molecular systems. In 1959 George and Griffith [41] had already drawn the attention to the superexchange mechanism in an attempt to interpret electron transfer in bridged metal ion complexes. This stimulated Halpern and Orgel [42] to calculate the promotion of electron transfer between metal ions by molecular bridges in the frame of superexchange. Later on and until today these metal complexes turned out to be ideal for the experimental demonstration of superexchange, especially since in such systems the mediating state can be directly observed in absorption spectroscopy [43].

In recent years the general importance of the superexchange mechanism for electron transfer processes in condensed phase has been recognized. In rigid or semirigid, covalently bridged donor-acceptor systems the electron transfer rate depends on the details of the electronic structure of the bridge [44–53]. Superexchange mechanisms are expected to operate also in systems where contact between donor, bridging species and acceptor is established by Van der Waals' interactions. By far the best defined rigid donor-medium-acceptor system with exclusively Van der Waals' contact between components is the photosynthetic reaction center, since the X-ray structure analysis gives the detailed position of both cofactors and amino acid residues.

In reaction centers the potential candidates for a specific role in superexchange interaction are aromatic systems located between donor and acceptor species. This follows from the fact that aromatic molecules exhibit lower reduction potentials relative to aliphatic systems, thus leading to smaller values of δE (Eqn. 1). This argument makes the involvement of the phytol chains a priori improbable. According to the primary sequences [54,55] and the X-ray structure analysis [1–7], the following aromatic groups structurally mediating between donors and acceptors are found in the reaction center of *Rb. sphaeroides* and *Rps. viridis*:

(a) Tyr-L162 between cytochrome and P may mediate the reduction of P^+. Replacement of this tyrosine by valine or lysine in site specific mutagenesis showed no loss of photochemical activity of RCs of *Rb. capsulatus* [56], the primary structure of which is strongly homologous [57] to *Rb. sphaeroides* and *Rps. viridis.*

(b) Tyr-M210 between P and H may mediate the primary electron transfer between $^1P^*$ and H. This amino acid residue is not conserved in the primary sequence of reaction centers of *Chloroflexus aurantiacus* [58–60]. Since the primary electron-transfer rate at room temperature is only by a factor of 3 slower [61,92] than the one observed for *Rb. sphaeroides* [12] and *Rps. viridis* [13], the role of this amino acid residue in superexchange is not expected to be predominant, although it may still contribute to the enhancement of the primary electron transfer rate.

(c) Trp-M252 between H and Q may mediate the Q reduction by H^-. This amino acid residue is conserved in the primary sequence of reaction centers of RCs as *Rb. sphaeroides* [53], *Rps. viridis* [55], *Rb. capsulatus* [57] and *Chloroflexus aurantiacus* [58–60] and might in a specific way contribute to the overall superexchange coupling through the protein.

(d) The accessory bacteriochlorophyll between P and H may mediate the primary electron transfer between $^1P^*$ and H across the A branch [23–33]. This cofactor seems to be conserved in all bacterial reaction centers characterized so far. In contrast to the amino acid residue, there is sufficient experimental evidence for a small value of δE, which is certainly much smaller than δE, as expected for aromatic amino acid residues.

A superexchange model employing the accessory bacteriochlorophyll to mediate electron transfer between $^1P^*$ and H will be analyzed in this paper. This model involves electronic coupling elements (V), energy differences (ΔG) and reorganization energies (λ), either extracted from experimental data (V, λ) or measured directly (ΔG). A set of parameters will be derived, which allows a consistent description of the primary electron transfer. Since a reliable and complete set of data is only available for RC's of *Rb. sphaeroides,* our analysis will be based on this species. Necessary structural information is borrowed from the available refined X-ray data at 2.3 Å resolution on reaction centers of *Rps. viridis* [1–3], and recent refined coordinates. This combination of data seems to be justified by the large extent of similarity in the 3-dimensional structures [1–7] which is consistent with the extensive homology of the primary sequences where the surrounding of the cofactors of the A branch tends to be conserved.

The superexchange mechanism

The primary electron transfer can be modelled in the framework of the nonadiabatic electron-transfer theory. The validity of this approximation is based on the observation that the experimental electron-transfer rate is slow as compared to the characteristic relaxation time of the protein medium. This relaxation time is proportional to the inverse effective average medium frequency which is approx. 100 cm^{-1} [87] and results in a relaxation time $\tau \approx 100$ fs. The rough estimate of $\tau \approx 100$ fs is consistent with recent molecular dynamics simulations of the protein structure in the RC accompanying electron transfer [63].

The basic equation for the electron-transfer rate is then given by [19,21,24,29,31,53,62,64,65,66]

$$k = \frac{2\pi}{\hbar} V^2 F \qquad (2)$$

where V is the electronic coupling and F is the thermally averaged nuclear Franck-Condon factor.

Consider first the nuclear contribution to k. The major contribution to F involves medium vibrational modes [62]. Under these circumstances F can be expressed within the effective single mode approximation. The full quantum mechanical expression for F assumes the form [64]

$$F = \frac{1}{\hbar\omega} \cdot e^{-S(2v+1)} I_p \cdot [2S \cdot \{v(v+1)\}^{1/2}] \cdot \left(\frac{v+1}{v}\right)^{p/2} \tag{3}$$

where

$$p = \frac{\Delta G}{\hbar\omega} \tag{4}$$

and

$$S = \frac{\lambda}{\hbar\omega} \tag{5}$$

ΔG is the free energy of the reaction, λ is the medium reorganization energy and ω is the (mean) vibrational frequency of the medium. The mean thermal vibrational excitation is

$$v = \frac{1}{e^{\hbar\omega/k_B T} - 1} \tag{6}$$

Finally, $I_p(\cdot)$ is the modified Bessel function of order p.

Provided that the frequencies of the nuclear modes, $\hbar\omega$, are sufficiently low relative to the thermal energy $k_B T$, the classical high-temperature limit of F is applicable, being given by the Marcus relation [65]

$$F = (4\pi\lambda k_B T)^{-1/2} e^{-E_a/k_B T} \tag{7}$$

where the activation energy E_a is given by

$$E_a = \frac{(\Delta G + \lambda)^2}{4\lambda} \tag{8}$$

Next, we consider the electronic coupling within the framework of the superexchange model. The superexchange electronic interaction between the lowest vibronic level of $^1P^*BH$, with the isoenergetic vibronic manifold of P^+BH^- is mediated by coupling with the state P^+B^-H. The effective coupling is composed of a direct and a superexchange contribution. The direct coupling will be neglected in the primary reaction, since it seems to be too small to be important in view of the large P–H distance (17Å for centre-to-centre separation) involved [1–7]. The superexchange coupling, Eqn. (I.1), V_{super}, assumes the form

$$V_{super} = \frac{V_{PB} V_{BH}}{\delta E} \tag{9}$$

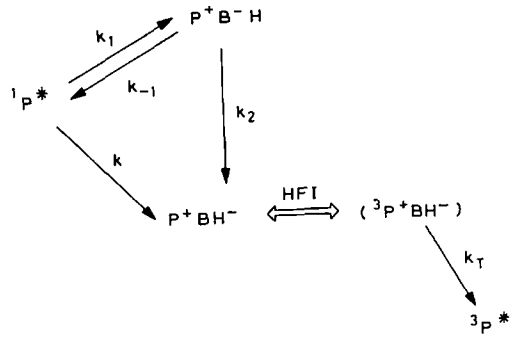

Fig. 2. Kinetic scheme for the competition between unistep superexchange and thermally activated sequential electron transfer in the RC. The formation and recombination of the $^3(P^+BH^-)$ radical pair is also shown.

where V_{PB} is the electronic coupling between $^1P^*BH$ and P^+B^-H, while V_{BH} is the electronic coupling between P^+B^-H and P^+BH^-. δE is the vertical energy difference between the potential surfaces for P^*BH and P^+B^-H at the intersection point of the potential surfaces of $^1P^*BH$ and P^+BH^- (Fig. 2).

Eqns. 2, 3 and 9 constitute the quantum-mechanical electron-transfer rate, which is valid for all temperatures, while the high-temperature limit of k is given by Eqns. 2, 7 and 9. The primary electron-transfer rate is activationless or pseudoactivationless [11,14,15,29], with the energetic parameters satisfying the relation $-\Delta G = \lambda$, i.e., $p = S$ (within $\pm$ 20%). The classical limit for the activationless rate is

$$k = \frac{2\pi |V_{super}|^2}{\hbar (4\pi\lambda k_B T)^{1/2}} \tag{10}$$

The procedure for the extraction of the parameters V and λ from experimental data using the electron transfer theory is outlined in Appendix I. The resulting quantities related to RC's of *Rb. sphaeroides* are:

$$\Delta G(^1P^*\text{-}P^+H^-) \approx -2000\ cm^{-1}$$

$$\lambda < 2500\ cm^{-1}$$

$$|V_{super}| \approx 25\ cm^{-1}$$

Information on the electronic coupling terms and the energetic parameter in Eqn. 5 is crucial to assess the validity of the superexchange mechanism. We have introduced [31] an intermolecular overlap approximation to calculate the relative magnitudes of the electronic coupling terms V_{PB} and V_{BH}. These calculations have determined the enhancement of the $B^-H\text{–}BH^-$ coupling over the $^1P^*B\text{–}P^+B^-$ coupling, with

$$\alpha = \left|\frac{V_{BH}}{V_{PB}}\right| \approx 6 \tag{11}$$

Indirect information on the vertical energy gap δE (Fig. 1) will be inferred from some kinetic constraints on the dynamics of the primary electron transfer [31,32], which were originally proposed by Marcus [66]. The present analysis is more detailed than previously given by us [31,32]. The superexchange model implies the existence of a parallel-activated electron-transfer channel. The experimental restrictions on the activated channel, such as undetectability of P^+B^- and temperature independence of the primary rate, provide the restrictions on the model parameters, electronic couplings and vertical energy differences.

The superexchange interaction between $^1P^*$ and P^+H^- requires the existence of the state P^+B^- with an energy, at the nuclear configuration of the transition state, which is higher than that of $^1p^*$ (Fig. 1). Such a state can also serve as an intermediate in a parallel-activated electron transfer according to the kinetic scheme of Fig. 2. The rate k_1 for the parallel activated transfer can be inferred from Eqns. 2, 7 and 8 and is given by

$$k_1 = \frac{2\pi}{\hbar}(4\pi\lambda_1 k_B T)^{-1/2} V_{PB}^2 \, e^{-(\Delta G_1 + \lambda_1)^2/4\lambda_1 k_B T} \tag{12}$$

where ΔG_1 is the free energy of P^+B^- relative to $^1P^*$ and λ_1 is the reorganisation energy in the activated process. In the vicinity of room temperature it is expected that the activated channel will contribute effectively to the observed rate.

The basic restriction on the kinetic scheme is the nondetectability of the intermediate state P^+B^- [33]. Taking into account the experimental uncertainties, the maximum concentration, $C = [P^+B^-]/[^1P^*]_0$ of P^+B^- relative to the initial concentration of $^1P^*$ should be $C \leq 0.10$ at room temperature and $C \leq 0.02$ at 10 K [14,15]. With the assumption $\lambda \geq 800\ cm^{-1}$, the lower bounds of acceptable parameters for the superexchange model were calculated in Ref. 33:

$$\delta E \geq 1100\ cm^{-1}$$

$$\Delta G_1 \geq 300\ cm^{-1}$$

$$V_{PB} \geq 60\ cm^{-1}$$

$$V_{BH} \geq 360\ cm^{-1} \tag{13}$$

A critical scrutiny of the energetics and individual electronic coupling terms emerging from the superexchange model is based on three sources: electric-field effects on the primary charge separation, the unidirectionality of charge separation across the A branch of the RC and magnetic interactions of the primary P^+H^- radical pair. These phenomena will be now considered within the framework of the superexchange mechanism.

Electric-field effects

The primary electron-transfer rate constant is affected by an external electric field, ϵ, through the shifts in the energies of the ion-pair states [67–72]. Two ion-pair states P^+B^- and P^+H^- are involved in the superexchange mechanism, whose dipole moments are

$$|\mu(P^+B^-)| = 51D$$

$$|\mu(P^+H^-)| = 82D$$

The orientation of the dipoles is given by the centre-to-centre vector for the corresponding ion pairs. The vertical energy gap, $\delta E(\epsilon)$, between $^1P^*$ and P^+B^- becomes [72]

$$\delta E(\epsilon) = \delta E(0) + \mu((P^+B^-)) \cdot \epsilon \tag{14}$$

The superexchange coupling, Eqn. (II.8), becomes field dependent

$$V_{super} = \frac{V_{PB} V_{BH}}{\delta E(0) + \mu(P^+B^-) \cdot \epsilon} \tag{15}$$

We assume [72] that the electronic coupling matrix elements V_{PB} and V_{BH} are independent of ϵ, as the field effect on the modification of the charge distribution of the ions will be exhibited only by second-order polarizability effects. The free energy, $\Delta G(\epsilon)$, of the electron transfer reaction is given by (see Ref. 72)

$$\Delta G(\epsilon) = \Delta G(0) - \mu(P^+H^-) \cdot \epsilon \tag{16}$$

and results in electric field dependence of the reduced energy parameter $p \equiv p(\epsilon)$, Eqn. 3, for the general case of the activation energy, Eqn. 8, for the high-temperature limit. The medium reorganization energy, λ, is assumed to be independent of the electric field, Eqns. 2 and 3, together with Eqns. 15 and 16, exhibit the field dependence of the primary electron-transfer rate, $k(\epsilon)$.

In a previous work [72], the field dependence of $k(\epsilon)$ was considered for oriented RC's. The primary rate is related to the fluorescence quantum yield $Y_f(\epsilon)$. For oriented RC's with a fixed direction of the electric field, the quantum yield is

$$Y_f(\epsilon) = \frac{k_d}{k(\epsilon) + k_d} \tag{17}$$

where k_d is the combined decay rate of $^1P^*$ in all radiative and nonradiative channels, excluding the charge separation channel.

Recent measurements of the field dependence of the fluorescence quantum yields [70] and of the fluorescence polarization [36] were performed in isotropic samples of RCs. In this case the angular distribution of the electron-transfer rates will originate from the continu-

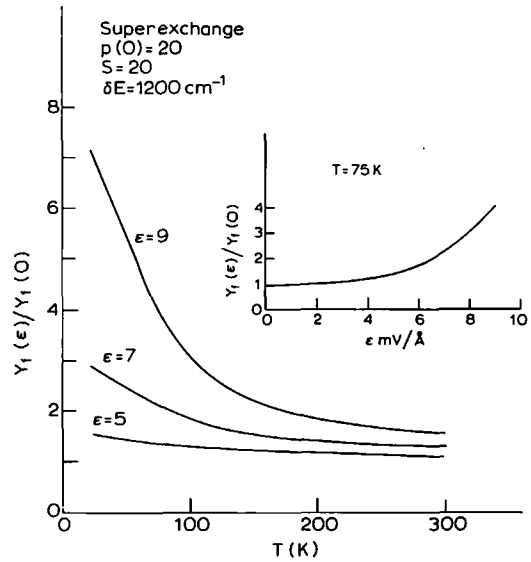

Fig. 3. The electric field and temperature dependence of the fluorescence quantum yields from isotropic samples over the temperature range 20–300 K, as calculated for the superexchange model. The electric field (ϵ) is given in units of mV/Å. The inset shows the electric field dependence at 75 K.

ous distribution of the orientation of the RCs with respect to the direction of the electric field. This angular spreading of the rate constant [72] in isotropic samples is reflected in the total fluorescence quantum yield, $Y_f(\epsilon) = \langle Y_f(\epsilon)\rangle$, where the averaging, $\langle\rangle$, is carried out over all the orientations of the RC with respect to the direction of the electric field [72]. Eqn. 17, together with the condition $k(\epsilon) \gg k_d$ for all relevant values of $|\epsilon|$, results in

$$\frac{Y_f(\epsilon)}{Y_f(0)} = k(0)\langle k(\epsilon)^{-1}\rangle \tag{18}$$

Fig. 3 displays the field dependence of the fluorescence quantum yield for isotropic samples, which was obtained applying the full quantum-mechanical expression, using the appropriate energetic parameters, Eqn. 13. Changing the parameters $p(0)$ and S within the permissible range of approx. 30%, which still leaves the process to be nearly activationless, leads only to a minor (up to 10%) modification of the total fluorescence quantum yield.

The electric field dependence of $Y_f(\epsilon)/Y_f(0)$ exhibits an increase of the relative fluorescence quantum yield with increasing ϵ and with lowering the temperature. The increase of $Y_f(\epsilon)/Y_f$ (0) becomes more pronounced at lower temperatures, reflecting the enhancement of the field-dependent F, Eqn. 3, with decreasing T. The predicted field dependence of $Y_f(\epsilon)$ should be confronted with the experimental data of Lockhart and Boxer [70], who find a modest increase of the fluorescence quantum yield $Y_f(\epsilon_E)/Y_f(0) = 1.25$ at 75 K for an external field of $\epsilon_E = 9$ mV/Å. The interrelationship between the externally applied field and the internal field requires a careful examination. Local field corrections, surface polarization effects and electrode contact effects, among others, have to be elucidated in this context [69]. The experimental result $Y_{f\epsilon_E=9mV/Å}/Y_f(0) = 1.25$ is close to the calculated value $Y_{f\epsilon=5mV/Å}/Y_f(0) = 1.39$ at 75 K. Although this agreement is not conclusive, as we have not established the relation between ϵ_E and ϵ, we may conclude that the field dependence of the fluorescence quantum yield is consistent with the superexchange mechanism.

Lockhart et al. [36] have pointed out that the measurements of the fluorescence polarization dependence at a constant electric field provide a more refined approach to distinguish between different mechanisms for the primary charge separation [30,33,17]. Under the assumption that optical excitation prepares the sample with an isotropic distribution of $^1P^*$ excited dimers, it is possible to model the polarization dependence of the fluorescence in the presence of an external electric field.

The yield $I_f(e, \epsilon)$ of the fluorescence with polarization in the direction $\mathbf{e}$, which is emitted from a given RC, is

$$I_f(e, \epsilon) = \alpha(e\cdot\mu_t)^2 \frac{k_d}{k_d + k(\epsilon)} \tag{19}$$

where α is a proportionality constant, μ is the transition dipole moment for the $P \rightarrow {}^1P^*$ excitation and $k(\epsilon)$ is the electron-transfer rate constant for the specific RC. The total fluorescence yield, $F(e, \epsilon)$, of radiation polarized in the e direction, is given by averaging $I_f(e, \epsilon)$ over all the possible orientations of the RC

$$F(e, \epsilon) = \alpha\langle(e\cdot\mu_t)^2 \frac{k_d}{k_d + k(\epsilon)}\rangle \simeq \alpha\langle(e\cdot\mu_t)^2 k_d/k(\epsilon)\rangle \tag{20}$$

At low fields $F(e\cdot\mu_t) \propto |\epsilon|$, the effects being linear in ϵ^2. It will be useful at this stage to define the angle χ between the polarization direction e and the external field ϵ, so that

$$F(e, \epsilon) \equiv F(\chi, \epsilon)$$

In view of the inherent difficulty in establishing the relation between ϵ and the external field one can consider the relative change of the polarized fluorescence Θ

$$\Theta(\chi) = \frac{F(\chi, \epsilon) - F(\epsilon = 0)}{F(\chi = 90°, \epsilon) - F(\epsilon = 0)} \tag{21}$$

which is independent of ϵ at sufficiently low fields.

Fig. 4 displays the calculated results for the relative change of the polarized fluorescence obtained for the superexchange mechanism. The calculations were performed using Eqn. (III.8) and utilizing the full quantum-mechanical expression for the electron-transfer rate

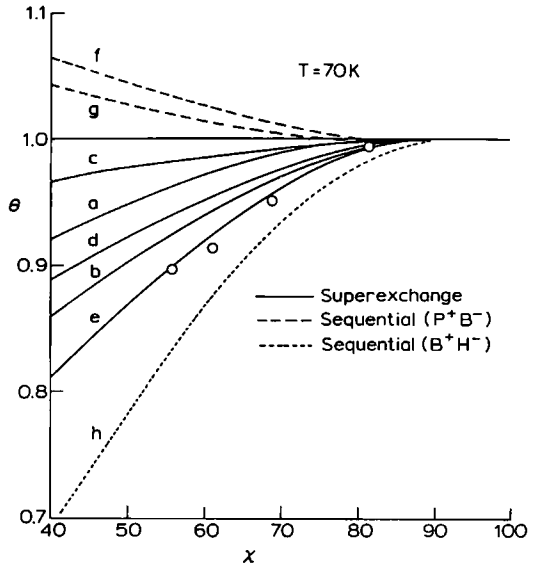

Fig. 4. The dependence of the relative polarized fluorescence $\Phi(\chi)$ on the angle χ between the polarization direction of the fluorescence and the electric field. Calculations were performed at 70 K. Superexchange model: solid curves (a)–(e); sequential model via P^+B^-: dashed curves (f) and (g); sequential model via PB^+H^-: dashed curve (h).

Curve	p	S	ψ	ϕ
(a)	20	20	58°	50°
(b)	20	16	58°	50°
(c)	20	24	58°	50°
(d)	20	20	61°	50°
(e)	20	16	61°	50°
(f)	10	8		50°
(g)	10	10		50°
(h)	10	10		80°

Open circles (○) represent the experimental data of Lockhart, Goldstein and Boxer (Ref. 36).

constant. The energetic input data were the zero-field energy gap, $\Delta G(0) = 2000\ cm^{-1}$, the medium reorganization energy $\lambda \leq 2400\ cm^{-1}$ and $\hbar\omega = 100\ cm^{-1}$ (Section The Superexchange Mechanism and Appendix I), which are consistent with activationless primary electron transfer. The geometric input information involves the angle ϕ between the transition moment μ_t and $\mu(P^+B^-)$ and the angle ψ between μ_t and μ (P^+B^-) and the angle ψ between μ_t and $\mu(P^+H^-)$. The available theoretical data [36] lead to the estimates $\phi = 50°$ and $\psi = 55°$–$61°$. Calculations were performed at 70 K although the temperature dependence of $\Phi(\chi)$ was found to be weak. As evident from Fig. 4, the calculated $\Phi(\chi)$ data for the superexchange mechanism are most sensitive to two parameters: the medium reorganization energy λ and the angle ψ, while the dependence of Φ on the angle ψ is very weak. In Fig. 4 we have also incorporated the experimental data for Φ obtained by Lockhart et al. [36] for reaction centers of *Rb. sphaeroides* at 70 K at moderately low external field of $\epsilon_E = 2$ mV/Å. Changing the energetic and angular parameters within their uncertainty range we find that Φ for the superexchange mechanism is close to the experimental results, with a good fit being accomplished for $\lambda = -1600\ cm^{-1}$ and $\psi = 61°$. We conclude that the superexchange mechanism is consistent with the field induced fluorescence polarization data [36].

At this point we would like to digress briefly on the predictions of other alternative sequential mechanisms for the primary charge separation [23,30,17]. In Fig. 4 we have included calculated results for $\Phi(\chi)$ for the sequential mechanism via P^+B^- with the equilibrium energy of the genuine intermediate P^+B^- state being located halfway in energy between $^1P^*$ and P^+H^-. The geometrical dependence of Φ in this mechanism is determined by the angle $\phi = 50°$, being independent of ψ. It is evident that this sequential mechanism is inconsistent with the experimental field induced fluorescence polarization data, in accord with the conclusions of Lockhart et al. [36]. The sequential mechanism through PB^+H^- [73] involved $\bar{\phi} = 80°$ which is the angle between $\mu(PB^+H^-)$ and μ_t. This mechanism results in a reasonable account of the experimental Φ data (Fig. 4). However, this sequential mechanism has inconsistencies with other experimental data [30,32,33].

Unidirectionality of charge separation

In sensitive measurements of the difference absorption in the Q_x band of H (Appendix II) the branching ratio of the primary rates across the A and B branches as measured for reaction centers of *Rb. sphaeroides* is [74]

$$\frac{k(A)}{k(B)} \geq 25 \quad \text{at 80 K} \tag{22}$$

We have attributed this remarkable effect of unidirectionality of the charge separation to structural symmetry breaking [29,31]. Evaluation of the electronic coupling term V_{PB} and V_{BH} across the A and the B branches of the RC demonstrated that small effects of structural asymmetry between P-B_A and P-B_B and between B_A-H_A and B_B-H_B modify the electronic coupling terms, which provide a central contribution to unidirectionality.

The intermolecular overlap approximation advanced and utilized by us resulted in the ratios [29,31]

$$\left|\frac{V_{PB}(A)}{V_{PB}(B)}\right|^2 = 7.7 \pm 3.8 \tag{23}$$

$$\left|\frac{V_{BH}(A)}{V_{BH}(B)}\right|^2 = 4.3 \pm 2.0 \tag{24}$$

resulting in the asymmetry of the electronic superexchange interaction

$$\psi = \left|\frac{V_{super}(A)}{V_{super}(B)}\right|^2 = \left|\frac{V_{PB}(A)}{V_{PB}(B)}\right|^2 \left|\frac{V_{BH}(A)}{V_{BH}(B)}\right|^2 \left|\frac{\delta E(A)}{\delta E(B)}\right|^2 \tag{25}$$

In the absence of experimental evidence regarding the vertical energy differences across the A and B branches we shall follow our previous analysis [29,31] and assume that the ratio $\delta E(A)/\delta E(B)$ is close to unity. Eqns. 22–24 then result in the asymmetry factor of the electronic coupling

$$\psi = 33 \pm 16 \tag{26}$$

The total asymmetry in the electron transfer rates $k(A)$ and $k(B)$ for charge separation across the A and B branches of the RC, respectively, is [29,31]

$$\frac{k(A)}{k(B)} = \psi r \tag{27}$$

where

$$r = \frac{F(A)}{F(B)} = \frac{F(\Delta G_A, \lambda, \omega)}{F(\Delta G_B, \lambda, \omega)} \tag{28}$$

is the ratio of the nuclear Franck-Condon factors. These are determined by the different free energy gaps ΔG_A and ΔG_B for the process (P^+BH^--$^1P^*BH$) across the A and B branches, respectively, and by the energetic parameters λ and ω, which are taken to be equal for the A and B branches. We have previously shown that the energetics of charge separation across the A and B branches is different, due to the extra stabilization of H_A^- by the polar Glu L104 residue. Simple electrostatic calculations (see Ref. 29) resulted in

$$\Delta_A - \Delta G_B = -720 \pm 320 \text{ cm}^{-1} \tag{29}$$

In Fig. 5 we summarize the dependence of r on P at 300 K and at 76 K calculated from the full quantum-mechanical expression over the range of the acceptable energetic parameters. The room temperature result (see Ref. 29) is

$$r = 1.35^{+0.35}_{-0.45} \quad (T = 300 \text{ K}) \tag{30}$$

while the low temperature result is

$$r = 2.5^{+3.1}_{-1.8} \quad (T = 80 \text{ K}) \tag{31}$$

Accordingly, the contribution of the nuclear Franck-Condon ratio r to the ratio $k(A)/k(B)$ is small. Our prediction [29] that $r = 1.35$ at 300 K is supported by the recent mutagenesis experiments. Exchange of the polar hydrogen-bonded Glu 104 against a Gln or Leu results only in a slight reduction of the primary rate by a numerical factor of about 1.4 [75].

The major contribution to the asymmetry of the rates originates from the electronic term. Eqn. 26 now predicts that for the superexchange mechanism the asymmetry is

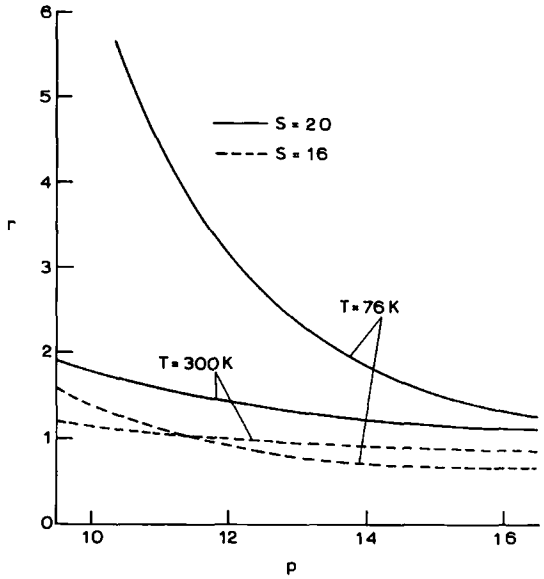

Fig. 5. The dependence of the ratio of the nuclear Franck Condon factors r on the energy gap p at $T = 76$ K and 300 K. Solid lines $S = 20$ and dashed lines $S = 16$.

$$\frac{k(A)}{k(rB)} = 45^{+38}_{-30} \quad (T = 300 \text{ K}) \tag{32}$$

and

$$\frac{k(A)}{k(B)} = 82^{+190}_{-70} \quad (T = 80 \text{ K}) \tag{33}$$

This result is in accord with the experimental value at 80 K, Appendix II. We have thus established the consistency of the superexchange mechanism with the structural symmetry breaking as the predominant reason for unidirectionality.

Magnetic interactions

The interrelationship between the primary electron-transfer kinetics in the RC and the properties of the radical pair P^+BH^-, such as the singlet-triplet splitting, J, and the triplet recombination rate, k_T, constitutes a long standing problem, which was recently addressed by several authors [22,32,33,76]. We shall show, following our recent study [32], that the properties of the radical pair can be accounted for within the framework of the superexchange model for the primary charge separation.

We shall consider the singlet-triplet splitting, K, of the radical pair and relate it to two kinetic rates: the

primary electron transfer rate, k, and the triplet recombination rate, k_T. The exchange interaction is

$$J = \delta E_S - \delta E_T \tag{34}$$

where δE_S and δE_T are the energy shifts of the singlet and triplet states of P^+BH^-, respectively. In principle, and in order to obtain the singlet and triplet shifts, one has to incorporate a large number of electronic states in the singlet and triplet manifolds, respectively. It is possible to obtain a general expression for the energy shifts by combining the partitioning method and first order perturbation theory to get

$$\delta E_\alpha = \sum_i \delta E_\alpha\{i\} \tag{35}$$

$$\delta E_\alpha\{i\} = -\frac{1}{E_v^\alpha(i) - E_v^\alpha(P^+H^-)} \times \left[\overline{V}_{i,P^+H^-} + \frac{\overline{V}_{i,P^+B^-}\overline{V}_{BH}(Q_\pm)}{E_v^\alpha(P^+B^-) - E_v^\alpha(P^+H^-)}\right]^2 \tag{36}$$

with the index $\alpha = S$ for singlet and $\alpha = T$ for triplet states. The sum over i refers to the (singlet or triplet) electronic states within several thousand cm^{-1} from P^+BH^-. The electronic coupling terms $\overline{V}_{ij}$ denote the matrix elements between the electronic states i and j in the equilibrium nuclear configuration $Q_\pm$ of the radical pair. Configurational relaxation of the prosthetic groups accompanying the formation of P^+BH^- may result in a new spatial arrangement of these prosthetic groups, which is different from the equilibrium configuration Q_0 of $^1P^*BH$. The vertical electronic energy $E_v^\alpha(i)$ of state i refers to nuclear equilibrium configuration $Q_\pm$. These are related to the equilibrium energies $E^\alpha(i)$ by $E_v^\alpha(i) = E^\alpha(i) + \lambda_i$, where λ_i is the medium reorganization energy of state i relative to P^+BH^-.

The calculation of the energy shifts δE_S and δE_T involves a large number of unknown reorganization energies and electronic coupling terms. In order to avoid proliferation of parameters, we shall calculate only the contributions of the dimer electronic excitations $^1P^*$ and $^3P^*$. As previously shown [32], these contributions constitute lower bounds for the energy shifts of the singlet and triplet states.

The direct first order contribution to the singlet shift $\delta E_s\{^1P^*\}$ is expected to be negligible; therefore we use only the superexchange contribution to Eqn. 36 which reduces to

$$\delta E_S\{^1P^*\} = -\left[\frac{\overline{V}_{BH}(Q_\pm)}{E_v(P^+B^-H) - E_v(P^+BH^-)}\right]^2 \times \frac{\overline{V}_{PB}(Q_\pm)^2}{E_v(^1P^*) - E_v(P^+BH^-)} \tag{37}$$

The singlet shift, Eqn. 37, can be related to the primary electron transfer rate, Eqns. 10 and (II.8), given by

$$k = \frac{2\pi}{\hbar}\left(\frac{V_{PB}V_{BH}}{\delta E}\right)^2 F \tag{38}$$

where in the high temperature limit, Eqn. 7 yields for the Franck-Condon factor

$$F = (4\pi\Delta G k_B T)^{-1/2} \tag{39}$$

Here ΔG is the (free) energy gap for the primary activationless process.

In order to relate $\delta E_S(^1P^*)$ to k we note that the matrix elements $\overline{V}_{BH}$ and $\overline{V}_{PB}$ correspond to the equilibrium nuclear configuration $Q_\pm$ of P^+BH^- while the matrix elements V_{PB} and V_{BH} correspond to the equilibrium nuclear configuration Q_0 of $^1P^*BH$. We have proposed [32] on the basis of recent molecular dynamics simulations of the RC [63] that the formation of the radical pair P^+BH^- results in a configurational relaxation of the bacteriopheophytin$^-$ (H^-) molecule. The main effect of such structural relaxation is assumed to be the reduction of $\overline{V}_{BH}(Q_\pm)$ relative to $V_{BH}(Q_0)$ and we set

$$\overline{V}_{BH} = bV_{BH} \tag{40}$$

where b (< 1) is a reduction factor. The V_{PB} electronic coupling is taken to be invariant, i.e., $\overline{V}_{PB} = V_{PB}$.

Eqns. 37–39 together with Eqn. 40 result in the following relationship between energetics and kinetics

$$\delta E_S\{^1P^*\} = -\frac{\hbar}{2\pi}kb^2\left\{\frac{\delta E^2 F^{-1}}{[E_v(^1P^*) - E_v(P^+H^-)][E_v(P^+B^-) - E_v(P^+H^-)]^2}\right\} \tag{41}$$

The relation between the singlet shift and k is rather complex because of two reasons. First, the energetic correction factor, which appears in the curly brackets in Eqn. 41, has to be taken into account. Secondly, the configurational relaxation reduction factor may be significant. Furthermore, the estimate of J cannot rely solely on the singlet contribution as the contribution of the triplet shift to Eqn. 34 is significant and must be incorporated.

To evaluate $\delta E_S\{^1P^*\}$ we use the following parameters: $\overline{V}_{PB} = V_{PB} = 65\ cm^{-1}$ and $\overline{V}_{BH} = bV_{BH}$ with $V_{BH} = 390\ cm^{-1}$ (Section The Superexchange Mechanism). For the singlet vertical energies we take $E_v(^1P^*) - E_v(P^+H^-) = \Delta G + \lambda$, with $\Delta G = 2000\ cm^{-1}$ and $\lambda = 1700\ cm^{-1}$, together with $E_v(P^+B^-H) - E_v(P^+BH^-) =$

2600 $cm^{-1} + \lambda$ with $\lambda = 1700\ cm^{-1}$. From this calculation we obtain

$$\delta E_S\{^1P^*\} = -1.0 \cdot 10^{-2}\, b^2\ (cm^{-1}) \tag{42}$$

We shall now proceed to the evaluation of the triplet energy shift, which according to Eqn. 36 is given by

$$\delta E_T\{^3P^*\} = -\frac{|{}^3V_{PH}^{eff}|^2}{E_v(^3P^*) - E_v(P^+H^-)} \tag{43}$$

where the effective coupling is

$${}^3V_{PH}^{(eff)} = {}^3\bar{V}_{PH} + \frac{{}^3\bar{V}_{PB}\,{}^3\bar{V}_{BH}}{E_v(P^+B^-) - E_v(P^+H^-)} \tag{44}$$

with the matrix elements corresponding to triplet electronic states in the nuclear configuration of $Q_{\pm}$.

The recombination rate of the triplet radical pair in *Rb. sphaeroides*, $^3P^+BH^- \rightarrow {}^3P^*$ is observed to be an activationless process with a rate constant $k_T \approx 5 \cdot 10^8\ s^{-1}$ and a free energy gap of $\Delta G_T = 1400\ cm^{-1}$ [77–79]. The activationless behavior of k_T indicates that the process takes place in approximately the equilibrium configuration of the radical pair $Q_{\pm}$, and one has to evaluate the relevant electronic coupling in this relaxed nuclear configuration. From the experimental information, with the help of Eqn. 11, it is possible to evaluate the triplet recombination rate

$$k_T = \frac{2\pi}{\hbar}|{}^3V_{PH}^{(eff)}|^2 F_T \tag{45}$$

with the effective electronic coupling ${}^3V_{PH}^{(eff)}$ consisting of a sum of direct and superexchange contributions being given by Eqn. 44. The high-temperature Franck-Condon factor is

$$F_T = (4\pi\Delta G_T k_B T)^{-1/2} \tag{46}$$

From Eqns. 43 and 45 we can establish a relation between the triplet energy shift and the triplet recombination rate

$$\delta E_T\{^3P^*\} = -\frac{(\hbar/2\pi)k_T F_T^{-1}}{E_v(^3P^*) - E_v(P^+H^-)} \tag{47}$$

Relation 47 constitutes a general model independent relation between δE_T and k_T, which is invariant with respect to the energetics of the P^{+-} state and to the mechanism of the primary charge separation. We shall now show that the triplet shift is large and must be incorporated in the evaluation of J, Eqn. 34.

The value of $|{}^eV_{PH}^{(eff)}| = 1.0\ cm^{+1}$ is estimated using Eqn. 45 from k_T for *Rb. sphaeroides* at 300 K. The triplet vertical energy gap appearing in Eqn. 43 is given by $E_v(^3P^*) - E_v(P^+BH^-) = \Delta G_T - \lambda_T = 1400\ cm^{-1} - \lambda_T$ where λ_T is the triplet reorganization energy for k_T. The triplet shift due to $^3P^*$ is

$$\delta E_T\{^3P^*\} = \frac{1}{1400 - \lambda_T}\ (cm^{-1}) \tag{48}$$

From the temperature independence of k_T [27] one can deduce that the reorganization energy λ_T is $\lambda_T \approx \Delta G_T$ (within 30%) where $\Delta G_T = 1400\ cm^{-1}$. Accordingly, $\lambda_T \leq 1800\ cm^{-1}$. For the upper limit of λ_T the energy shift is $\delta E_T\{^3P^*\} = -2.5 \cdot 10^{-3}\ cm^{-1}$. If λ_T is smaller than $1800\ cm^{-1}$ but still larger than $1400\ cm^{-1}$, $\delta E_T\{^3P^*\} < -2.5 \cdot 10^{-3}\ cm^{-1}$. When $1000\ cm^{-1} < \lambda_T < 1400\ cm^{-1}$ Eqn. 43 results in $\delta E_T\{^3P^*\} \geq 2.5 \cdot 10^{-3}\ cm^{-1}$. We conclude that for the acceptable values of λ_T $|\delta E_T(^3P^*)| \geq 2.5 \cdot 10^{-3}\ cm^{-1}$, which exceeds the experimental value of $|J| = 10^{-3}\ cm^{-1}$ for *Rb. sphaeroides* [34,81–83]. As the estimate of $\delta E_T\{^3P^*\}$ is model independent, we conclude that for $1000 < \lambda_T < 1400\ cm^{-1}$ the positive triplet shift $\delta E_T\{^3P^*\} \geq 2.5 \cdot 10^{-3} cm^{-1}$ will add up to the value of δE_S, Eqn. 34, and the resulting absolute value of J would be therefore larger than $2.5 \cdot 10^{-3}\ cm^{-1}$, in contrast to the small experimental value of $|J|$. Consequently, we must conclude that $\lambda_T > 1400\ cm^{-1}$, with an acceptable value being $\lambda_T = 1800\ cm^{-3}$, which leads to $\delta E_T\{^3P^*\} \leq -2.5 \cdot 10^{-3} cm^{-1}$.

We shall subsequently utilize $\delta E_S\{^1P^*\}$ and $\delta E_T\{^3P^*\}$ to represent the upper bounds for δE_S and δE_T, respectively. Our final estimate of the singlet-triplet splitting of the P^+BH^- radical pair is then

$$J = (-1.0 \cdot 10^{-2}\, b^2 + 2.5 \cdot 10^{-3}) cm^{-1} \tag{49}$$

This estimate of J rests on the superexchange mechanism for the evaluation of δE_S and a self-consistency relationship between experimental kinetic (k_T) and magnetic (J) data for δE_T. Two features of the expression for J, Eqn. 49 are noteworthy:

(1) the appearance of the square of the reduction factor b^2 which manifests configurational relaxation of the prosthetic groups in the P^+B^- state; and

(2) the essential cancellation between the singlet and triplet contributions which can be traced to the large, model independent, value of δE_T.

Both effects may result in a diminishing of the calculated value of $|J|$. Reduction parameters in the range $0.40 < b < 0.6$ give J values in the range $J = -1.1 \cdot 10^{-3}$ to $J = +0.9 \cdot 10^{-3}\ cm^{-1}$, in accord with the experimental result $|J| \approx 10^{-3}\ cm^{-1}$ for *Rb. sphaeroides*.

The triplet recombination rate k_T

One of the interesting kinetic features of the reaction center is the large difference between the primary rate k, Eqns. 38 and 39, and the triplet recombination rate

k_T, Eqns. 45 and 46. The experimental data give $k/k_T \approx 650$ for quinone-free reaction centers of *Rb. sphaeroides* [27]. Since both reactions are activationless, this ratio of rates corresponds to the ratio

$$\frac{k}{k_T} = \left| \frac{V_{super}}{{}^3V_{BH}^{(eff)}} \right|^2 \frac{F_T}{F} \tag{50}$$

As the medium reorganization energies are close, i.e., $\lambda \approx 2000 \pm 400$ cm^{-1} and $\lambda_T \approx 1800$ cm^{-1} the ratio of the Franck-Condon factors, Eqns. (V.6) and (V.13) is close to unity, so that $k/k_T = \left| V_{super}/{}^3V_{BH}^{(eff)} \right|^2$ and the ratio of the electronic couplings is

$$\frac{V_{super}}{{}^3V_{BH}^{(eff)}} = \left(\frac{k}{k_T} \right)^{1/2} = 25 \tag{51}$$

The triplet coupling ${}^3V_{BH}^{(eff)}$, Eqn. 34, contains both direct and superexchange contributions. We assume that the superexchange contribution to k_T is comparable to or larger than the direct coupling, and we approximate ${}^3V_{BH}^{(eff)}$ by the superexchange contribution. Utilizing Eqns. 9 and 44 the ratio of the two couplings in Eqn. 51 is given by

$$\left(\frac{k}{k_T} \right)^{1/2} = \frac{V_{PB} V_{BH} \Delta E_v}{{}^3\overline{V}_{PB} {}^3\overline{V}_{BH} \delta E} \tag{52}$$

where $\Delta E_v = E_v(P^+B^-H) - E_v(P^+BH^-)$.

Eqn. 52 contains the matrix elements ${}^3\overline{V}_{PB}$ and ${}^3\overline{V}_{BH}$ which should be computed in the nuclear equilibrium configuration of P^+BH^-, while the matrix elements V_{PB} and V_{BH} correspond to the nuclear equilibrium configuration of ${}^1P^*BH$. The ${}^3\overline{V}_{BH}$ coupling between ${}^3(P^+B^-H)$ and ${}^3(P^+BH^-)$ is expected to be close to the corresponding singlet coupling $\overline{V}_{BH}$, which in turn is related to V_{BH} by Eqn. 40, so that ${}^3\overline{V}_{BH} = bV_{BH}$. The ${}^3\overline{V}_{PB}$ triplet coupling between ${}^3P^*BH$ and ${}^3(P^+B^-H)$ is expected to differ from the corresponding singlet $\overline{V}_{PB} \approx V_{PB}$ interaction between ${}^1P^*BH$ and P^+B^-H in view of the difference between the electronic part of the wavefunctions of ${}^3P^*$ and of ${}^1P^*$. Quantum mechanical computations on the RC of *Rps. viridis* [84] show that ${}^1P^*$ is highly polar with an excess electron charge of $\delta \approx 0.5e$ being localized on P_B which is closer to B_A than to B_B. This charge asymmetry enhances the electronic coupling V_{PB} across the A branch [29,31]. This charge asymmetry will also enhance $\overline{V}_{PB}$ at the nuclear configuration $Q_{\pm}$. In contrast, such a pronounced charge asymmetry is experimentally not detected for the ${}^3P^*$ state. The differences in the electronic wavefunctions of ${}^1P^*$ and ${}^3P^*$ affect the intermolecular coupling between the electronic excitation of the dimer and the P^+B^-, which appear in Eqn. 52. We shall take ${}^3\overline{V}_{PB} = \eta\overline{V}_{PB} = \eta V_{PB}$ where η represent a charge asymmetry parameter, which on the basis of theoretical [84] and ESR data [85,86] is expected to be $\eta < 1$. Eqn. 52 now results in

$$\left(\frac{k}{k_T} \right)^{1/2} = (\eta b)^{-1} \frac{\Delta E_v}{\delta E} \tag{53}$$

Taking $\Delta E_v = 4500$ cm^{-1} and $\delta E = 1200$ cm^{-1} together with $(k/k_T)^{1/2} = 25$ results in the product of the structural and electronic reduction parameters $\eta b = 0.2$. From the foregoing estimate of b (Section Magnetic interactions) we have tentatively inferred the values $0.4 < b < 0.6$, which result in $0.35 < \eta < 0.50$.

Concluding remarks

We have demonstrated that a number of physical phenomena and observables can be accounted for and are consistent with the superexchange mechanism for the primary electron transfer in the reaction center of *Rb. sphaeroides*. These include electric-field effects on the quantum yield and polarization of the prompt fluorescence, the exchange integral and the triplet recombination rate of the primary radical pair P^+H^- and the unidirectionality of the charge separation across the A-branch. Such a consistency check provides, of course, a necessary but insufficient condition for the validity of the superexchange model.

Our analysis requires some plausible but ad hoc assumptions in order to explain the experimental recombination parameters J and k_T. It is assumed that the formation of P^+H^- is accompanied by a configurational relaxation of protein and cofactors upon which the coupling V_{BH} is reduced. The second assumption implies that the electronic coupling involving the triplet state ${}^3P^*$ are smaller than the ones involving the singlet state ${}^1P^*$.

It is important to note that the full consistent description of the primary charge separation includes an activated sequential electron-transfer channel (Eqn. II.11) in parallel to the direct superexchange pathway. At high temperatures the contribution of the activated channel may be significant.

Appendix I. Extraction of parameters involved in electron transfer rates

The electron-transfer rate in the nonadiabatic, effective single-mode approximation is characterized by the following set of parameters:

(1) Δ, the reaction free energy;
(2) λ, the medium reorganisation energy;
(3) ω, the effective average frequency of the medium;
(4) V, the electronic coupling responsible for the electron transfer.

The quantum-mechanical expression for the rate is given by Eqn. 3 in terms of the dimensionless free

energy $p = \Delta G/\hbar\omega$ and the dimensionless reorganization energy $S = \lambda/\hbar\omega$. The classical limit of the rate can be obtained as a limiting behaviour of Eqn. 3 under the condition $\hbar\omega \ll k_B T$ as given by Eqns. 3–8 [65].

Two of the parameters involved in the rate constant can be obtained from independent measurements. Those are ΔG and the effective frequency which is taken as the average of the low-frequency band of the protein [87]. The value that we are using is $\hbar\omega = 100\ cm^{-1}$ [62]. The high-frequency modes only renormalize the electronic coupling through the Franck-Condon factors.

The parameters λ can be obtained only from the analysis of the temperature dependence of the rate constant according to Eqn. 3. The problem is simplified somehow if the rate constant is activationless (or pseudo-activationless). If experiments show that the rate constant remains constant within a factor of 2 in the temperature range 300 K–4 K, one may conclude that $\lambda \leq -1.3\ \Delta G$. This analysis takes into account the possible transitions to excited vibrational states in the inverted region, and neglects changes in the electronic coupling, V, due to possible changes in the nuclear coordinates of the protein.

The knowledge of ΔG, λ and $\hbar\omega$ allows the solution of Eqn. 2 for the electronic V.

Appendix II. A new limit for the ratio $k(A)/k(B)$

In RC's *R. sphaeroides* R-26 the Q_x absorption bands of the two bacteriopheophytins split at low temperatures showing absorption peaks at $\lambda = 546$ nm for H_A and $\lambda = 531$ nm for H_B [88–90]. Fig. 6 shows the bleaching spectrum in the range of the Q_x absorption of H_A and H_B at times longer than 40 ps. While H_A exhibits a bleaching of 190 milli absorbance units (mA), the range between 526 nm and 536 nm is essentially flat. The amplitude of the residual structure is smaller than 7.5 milli absorbance units (mA). This ratio of the bleachings limits the ratio of the yields, $\Phi(H_A)/\Phi(H_B) > 25$, which corresponds to the ratio $k(A)/k(B)$ [74].

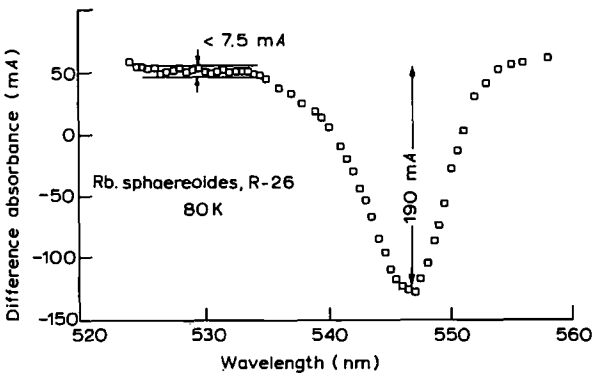

Fig. 6. Difference absorbance spectrum at 90 K of RC's of *Rb. sphaeroides* R-26, excited at 600 nm (excitation probability ≈ 70%) probed at maximum overlap in time (width of laser pulses, 40 ps). Sample: 35 μM RC in 0.08% LDAO, 20 mM Tris-HCl, (pH 8.0) 65% glycerol in a 5 mm cuvette.

Acknowledgement

This research was supported by the Deutsche Forschungsgemeinschaft (SFB 143).

References

1 Deisenhofer, J., Epp, O., Miki, K., Huber, R. and Michel, H. (1984) J. Mol. 180, 385–398.
2 Deisenhofer, J., Epp, O., Miki, K., Huber, R. and Michel, H. (1986) Nature 318, 618–624.
3 Michel, H., Epp, O. and Deisenhofer, J. (1986) EMBO J. 5, 2445–2451.
4 Allen, J.P., Feher, G., Yeates, T.O., Rees, D.C., Deisenhofer, J., Michel, H. and Huber, R. (1986) Proc. Natl. Acad. Sci. USA 83, 8589–8593.
5 Chang, C.H., Tiede, D., Tang, J., Smith, U., Norris, J. and Schiffer, M. (1986) FEBS Lett. 205, 82–86.
6 Allen, J.P., Feher, G., Yeates, T.O., Komiya, H. and Rees, D.C. (1987) Proc. Natl. Acad. Sci. USA 84, 5730–5734.
7 Allen, J.P., Feher, G., Yeates, T.O., Komiya, H. and Rees, D.C. (1987) Proc. Natl. Acad. Sci. USA 84, 6162–6166.
8 Norris, J.R., Uphaus, R.A., Crespi, H.L. and Katz, J.J. (1971) Proc. Natl. Acad. Sci. USA 68, 625–628.
9 Feher, G., Hoff, A.J., Isaacson, R.A. and Ackerson, L.C. (1975) Ann. N.Y. Acad. Sci. 244, 239–259.
10 Rockley, M.G., Windsor, M.W., Cogdell, R.J. and Parson, W.W. (1975) Proc. Natl. Acad. Sci. USA 72, 2251–2255.
11 Kaufmann, K.J., Dutton, P.L., Netzel, T.A., Leigh, J.S. and Rentzepis, P.L. (1975) Science 188, 1301–1304.
12 Martin, J.L., Breton, J., Hoff, A.J., Migus, A. and Antonetti, A. (1986) Proc. Natl. Acad. Sci. USA 83, 957–961.
13 Breton, J., Martin, J.-L., Migus, A., Antonetti, A. and A. Orszag (1986) Proc. Natl. Acad. Sci. USA 83, 5121–5125.
14 Martin, J.-L., Breton, J., Lambry, J.C. and Fleming, G.R. (1988) in: The Photosynthetic Bacterial Reaction Center. Structure and Dynamics. (Breton, J. and Verméglio, A., eds.), pp. 195–203. NATO ASI series, Plenum, New York.
15 Fleming, R.G., Martin, J.-L. and Breton, J. (1988) Nature 333, 190–192.
16 Parson, W.W., Woodbury, N.W.T., Becker, M., Kirmaier, C. and Holten, D. (1985) in: Antennas and Reaction Centers of Photosynthetic Bacteria (Michel-Beyerle, M.E., ed.), pp. 278–285, Springer, Berlin.
17 Marcus, R.A. (1988) Isr. J. Chem. 28, 205–213.
18 Haberkorn, R., Michel-Beyerle, M.E. and Marcus, R.A. (1979) Proc. Natl. Acad. Sci. USA 70, 4185–4188.
19 Marcus, R.A. (1987) Chem. Phys. Lett. 133, 471–477.
20 Chekalin, S.V., Matveetz, Ya.A., Shkuropatov, A.Ya., Shuvalov, V.A. and Yartzev, A.P. (1987) FEBS Lett. 216, 245–248.
21 Fischer, S.F. and Scherer, P.O.J. (1987) Chem. Phys. 115, 151–158.
22 Marcus, R.A. (1988) Chem. Phys. Lett. 146, 13–22.
23 Woodbury, N.W., Becker, M., Middendorf, D. and Parson, W.W. (1985) Biochemistry 24, 7516–7521.
24 Fischer, S.F., Nussbaum, I. and Scherer, P.O.J. (1985) in: Antennas and Reaction Centers of Photosynthetic Bacteria, (Michel-Beyerle, M.E., ed.), pp. 256–263, Springer, Berlin.
25 Jortner, J. and Michel-Beyerle, M.E. (1985) in: Antennas and Reaction Centers of Photosynthetic Bacteria, (Michel-Beyerle, M.E., ed.), pp. 345–365, Springer, Berlin.
26 Jortner, J. and Bixon, M. (1987) in: Protein Structure Molecular and Electronic Reactivity (Austin, R., Buhks, E., Chance, B.,

DeVault, D., Dutton, P.L., Frauenfelder, H. and Gol'danskii, V.I. eds.), pp. 277–308, Springer-Verlag, New York.
27 Ogrodnik, A., Remy-Richter, N., Michel-Beyerle, M.E. and Feick, R. (1987) Chem. Phys. Lett. 135, 576–581.
28 Norris, J.R., Budil, D.E., Tiede, D.M., Tang, J., Kolaczkowski, S.V., Chang, C.H. and Schiffer, M. (1987) in Progress in Photosynthesis Research (Biggins, J., ed.), Vol. I, pp. 363–369, Martinus Nijhoff, Dordrecht.
29 Michel-Beyerle, M.E., Plato, M., Deisenhofer, J., Michel, H., Bixon, M. and Jortner, J. (1988) Biochim. Biophys. Acta 932, 52–70.
30 Bixon, M., Jortner, J., Plato, M. and Michel-Beyerle, M.E. (1988) in: The Photosynthetic Bacterial Reaction Center. Structure and Dynamics. (Breton, J. and Verméglio, A., eds.), pp. 399–420 NATO ASI series, Plenum, New York.
31 Plato, M., Möbius, K., Michel-Beyerle, M.E., Bixon, M. and Jortner, J. (1988) J. Am. Chem. Soc., 110, 9279–9285.
32 Michel-Beyerle, M.E., Bixon, M. and Jortner, J. (1988) Chem. Phys. Lett. 151, 188–194.
33 Bixon, M., Michel-Beyerle, M.E. and Jortner, J., (1988) Isr. J. Chem. 28, 155–168.
34 Hunter, D.A., Hoff, A.J. and Hore, P.J. (1987) Chem. Phys. Lett. 134, 6–11.
35 Bixon, M., Jortner, J., Michel-Beyerle, M.E., Ogrodnik, A. and Lersch, W. (1987) Chem. Phys. Lett. 140, 626–630.
36 Lockart, D.J., Goldstein, R.F. and Boxer, S.G. (1988) J. Chem. Phys. 89, 1408–1415.
37 Kramers, H.A. (1934) Physica 1, 182–193.
38 Shull, C.G., Stauser, W.A. and Wollan, E.O. (1951) Phys. Rev. 83, 333–349.
39 Anderson, P.W. (1959) Phys. Rev. 115, 2–31.
40 McConnel, H.M. (1961) J. Chem. Phys. 35, 508–515.
41 George, M. and Griffith, J.S. (1959) in: The Enzymes, 1, pp. 347–392, Academic Press, New York.
42 Halpern, J. and Orgel, L.E. (1960) Disc. Farad. Soc. 29, 32–41.
43 Richardson, D.E. and Taube, H. (1983) J. Am. Chem. Soc. 105, 40–51.
44 Joran, A.D., Leland, B.A., Geller, G.G., Hopfield, J.J. and Dervan, P.B. (1984) J. Am. Chem. Soc. 106, 6090–6092.
45 Miller, J.R. (1985) in: Antennas and Reaction Centers of Photosynthetic Bacteria (Michel-Beyerle, M.E., ed.), pp. 234–241, Springer Berlin.
46 Heitele, H. and Michel-Beyerle, M.E. (1985) in: Antennas and Reaction Centers of Photosynthetic Bacteria, (Michel-Beyerle, M.E., ed.), pp. 250–255, Springer, Berlin.
47 Beratan, D.N. (1986) J. Am. Chem. Soc. 108, 4321–4326.
48 Heitele, H. and Michel-Beyerle, M.E. (1987) Chem. Phys. Lett. 134, 273–278.
49 Warman, J.M., De Haas, M.P., Paddon-Row, M.N., Cotsaris, E., Hush, N.S., Oevering, H. and Verhoeven, J.W. (1986) Nature 320, 615–616.
50 Larsson, S. and Volosov, A. (1986) J. Chem. Phys. 85, 2548–2553.
51 Closs, G.L., Calcaterra, L.T., Green, N.J., Penfield, K.W. and Miller, J.R. (1986) J. Phys. Chem. 90, 3672–3683.
52 Ohta, K., Closs, G.L., Morokuma, K. and Green, N.J. (1986) J. Am. Chem. Soc. 108, 1319–1320.
53 Closs, G.L. and Miller, J.R. (1988) Science 140, 440–447.
54 Williams, J.C., Steiner, L.A. and Feher, G. (1986) Proteins: Structure, Function and Genetics 1, 312–325.
55 Michel, H., Weyer, K.A., Gruenberg, H., Dunger, I., Oesterhelt, D. and Lottspeich, F. (1986) EMBO J. 5, 1149–1158.
56 Bylina, E.J., Jovine, R. and Youvan, D.C. (1988) in: The Photosynthetic Bacterial Reaction Center (Breton, J. and Verméglio, A., eds.), NATO ASI Series 149, pp. 113–118, Plenum Press, New York.
57 Youvan, D.C., Bylina, E.J., Alberti, M., Begusch, H. and Hearst, J.E. (1984) Cell 37, 949–557.
58 Ovchinnikov, Yu.A., Abdulaev, N.G., Zolotarev, A.S., Shmukler, B.E., Zargarov, A.A., Kutuzov, M.A., Telezhinskaya, I.N. and Levine, N.B. (1988) FEBS Lett. 232, 237–242.
59 Ovchinnikov, Yu.A., Abdulaev, N., Shmukler, B.E., Zargarov, A.A., Kutuzov, M.A., Telezhinskaya, I.N., Levina, N. and Zolotarev, A.S. (1988) FEBS. Lett. 232, 364–368.
60 Shiozawa, J.A., Lottspeich, F. and Feick, R., Eur. J. Biochem., in press.
61 Becker, M., Middendorf, D., Woodbury, N.W., Parson, W.W. and Blankenship, R.E. (1986) in: Ultrafast Phenomena V (Fleming, G.R. and Siegman, A.E., eds.), pp. 374–378, Springer Berlin.
62 Bixon, M. and Jortner, J. (1986) J. Phys. Chem. 90, 3795–3800.
63 Treutlein, H., Schulten, K., Deisenhofer, J., Michel, H., Brunger, A. and Karplus, M. in: The Photosynthetic Bacterial Reaction Center. Structure and Dynamics. (Breton, J. and Verméglio, A., eds.), pp. 139–150, NATO ASI series, Plenum, New York.
64 Jortner, J. (1976) J. Chem. Phys. 64, 4860–4867.
65 Marcus, R.A. (1956) J. Chem. Phys. 24, 966–978 and 979–989.
66 Marcus, R.A. (1988) in: The Photosynthetic Bacterial Reaction Center (Breton, J. and Verméglio, A., eds.), NATO ASI Series A 149, pp. 389–398 Plenum Press, New York.
67 Popovic, Z.D., Kovacs, G.J., Vincett, P.S., Alegria, G. and Dutton, P.L. (1986) Chem. Phys. 110, 227–237.
68 Gopher, A., Blatt, Y., Schönfeld, M., Okamura, M.Y., Feher, G. and Montal, M. (1985) Biophys. J. 48, 311–320.
69 Feher, G., Arno, T. and Okamura, M.Y. (1988) in: The Photosynthetic Reaction Center (Breton, J. and Verméglio, A., eds.), NATO ASI Series A 149, pp. 271–287, Plenum Press New York 1988.
70 Lockhart, D.J. and Boxer, S.G. (1988) Chem. Phys. Lett. 144, 243–249.
71 Popovic, Z.D., Kovacs, G.J., Vincett, P.S., Alegria, G. and Dutton, P.L. (1986) Biochim. Biophys. Acta 851, 38–48.
72 Bixon, M. and Jortner, J. (1988) J. Phys. Chem. 92, 7148–7156.
73 Scherer, P.O.J. and Fischer, S.F. (1987) Chem. Phys. 115, 151–158.
74 Aumaier, W., Eberl, U., Ogrodnik, A. and Michel-Beyerle, M.E. (1989) in Progress in Photosynthesis Research, in press
75 Bylina, E.J., Kirmaier, C., McPowell, L., Holten, D. and Youvan, D.C. (1988) Nature 336, 182–184.
76 Won, Y. and Friesner, R.A. (1988) Biochim. Biophys. Acta 935, 9–18.
77 Agrodnik, A., Volk, M. and Michel-Beyerle, M.E. (1988) in: The Photosynthetic Reaction Center (Breton, J. and Verméglio, A., eds.), NATO ASI Series A 149, pp. 177–183, Plenum Press, New York.
78 Ogrodnik, A., Vol, M., Letterer, R., Feick, R. and Michel-Beyerle, M.E. (1988) Biochim. Biophys. Acta, 936, 361–371.
79 Goldstein, R.A., Takiff, L. and Boxer, S.G. (1988) Biochim. Biophys. Acta 934, 253–263.
80 Hoff, A.J. (1986) Photochem. Photobiol. 43, 727–745.
81 Volk, M., Scheidel, G., Ogrodnik, A., Feick, R. and Michel-Beyerle, M.E. (1989) in Progress in Photosynthesis Research, in press.
82 Lersch, W., Lendzian, F., Lang, E., Feick, R., Möbius, K. and Michel-Beyerle, M.E. J. Magn. Res.
83 Lersch, W., Lang, E., Feick, R. and Michel-Beyerle, M.E. (1989) Perspectives in Photosynthesis (Pullman, B. and Jortner, J., eds.), Reidel, Dordrecht, in press.
84 Plato, M., Lendzian, F., Lubitz, W., Traenkle, E. and Moebius, K. (1988) in: The Photosynthetic Bacterial Reaction Center, Structure and Dynamics (Breton, J. and Verméglio, A., eds.), NATO ASI Series A: Life Sciences, 149, 379–388, Plenum Press New York.
85 Norris, J.R., Budil, D.E., Crespi, H.L., Bowman, M.K., Gast, P., Lin, L.P., Chang, C.H. and Schiffer, M. (1985) in: Antennas and Reaction Centers of Photosynthatic Bacteria (Michel-Beyerle, M.E., ed.), pp. 147–149, Springer Verlag.
86 Gast, P., deGroot, A. and Hoff, A.J. (1983) Biochim. Biophys. Acta 723, 52–61.

88 McElroy, J.D., Mauzerall, D.C. and Feher, G. (1974) Biochim. Biophys. Acta 333, 261–268.
89 Kirmaier, C., Holten, D., Parson, W.W. (1985) Biochim. Biophys. Acta 810, 49–61.
90 Volk, M., Ogrodnik, A., Feick, R. and Michel-Beyerle, M.E. (1989) in Progress in Photosynthesis Research, in press.
91 Creighton, S., Hwang, J.-K., Warshel, A., Parson, W.W. and Norris, J. (1988) Biochemistry 27, 774–781.
92 Kirmaier, C., Blankenship, R.E. and Holten, D. (1986) Biochim. Biophys. Acta 850, 275–285.
93 Gō, N., Noguti, T. and Nishikawa, T. (1983) Proc. Natl. Acad. Sci. USA 80, 3696–3700.